Reduced-Loss PWM Strategy For Three-Phase Voltage-Type Inverters

R.N.C. Alves, E.R.C. da Silva, A.M.N. Lima, and C.B. Jacobina
Laboratório de Eletrônica Industrial e Acionamento de Máquinas
Departamento de Engenharia Elétrica, Universidade Federal da Paraíba
58109-970 Campina Grande, PB, Brasil, Caixa Postal 10.105
Fax: ++55-83-3101015 Email: edison@dee.ufpb.br

***Abstract* - The performance characteristics of different PWM strategies are examined in terms of the amplitude of the ripple current as a function of the apportioning factor. Also the influence of the power angle on losses is taken into account as a function of such apportioning factor. A hybrid modulator scheme that allows to generate any continuous or discontinuous PWM has been implemented. Selected simulation and experimental results to demonstrate the validity of the proposed technique are presented.**

I. INTRODUCTION

In AC motor drive, a given converter voltage Space Vector Modulation (SVM) can be realized by a three-phase PWM voltage converter by switching either three bridge legs (*continuous modulation)* or two bridge legs (*discontinuous modulation*). In the discontinuous modulation the third phase is clamped to the positive or negative DC link [1–4]. Identical results can be obtained from carrier based PWM techniques. In these techniques (e.g. Sinusoidal Modulation, SM) [5], the discontinuous PWM modulation can be obtained by adding a zero sequence component, *zsc*, to the three sinusoidal reference voltages. As a consequence, the modulating signals are non-sinusoidal (NSMS) [6, 7]. In both cases there is an improvement in the waveform quality and an increase in the effective system frequency, while the linearity region of the PWM strategy is extended for about 15.5% [3,6,8,9]. As a result the waveform of the ripple voltage and the amplitude of the ripple current are affected. These strategies are related because the addition of zero sequence components into the PWM waveform controls the placement of the null space vector within the modulation period [8] and *vice-versa*. References [9, 10] have developed algorithms based on the apportioning factor of the null vector time that are suitable for microprocessor and analog implementation. In [11] the modulator scheme consists of simple logic blocks, and allows a systematic and straight approach to generate any continuous or discontinuous PWM. On the other hand, in order to minimize the losses, some PWM schemes have been developed [3,12,13], in which variable clamped segments are distributed according to the power angle, between output voltage and current. Among them, only the strategy presented in [13] guarantees the minimization of switching loss in all the range of the phase angle.

In this paper the performance characteristics of different PWM strategies are examined in terms of the amplitude of the ripple current as a function of the apportioning factor. By adapting the strategy presented in [13] the influence of the power angle on losses is taken into account as a function of such apportioning factor. These techniques are easily implemented by a hybrid modulator scheme that allows a systematic and straight approach to generate any continuous or discontinuous PWM strategy. Simulated and experimental results demonstrate the validity of the proposed technique.

II. BACKGROUND

The introduction of a zero sequence component, v_h, in a modulator does not affect the inverter line to line voltage, but significantly influences the switching frequency characteristics. Also, in SVM the split and distribution of the duration of the zero-state vectors (see Fig. 1) V_0 and V_7 at the beginning, t_{o1}, and at the end, t_{o2}, of the sampling interval, respectively, can be represented by the apportioning factor $\mu = t_{o1}/(t_{o1} + t_{o2})$.

It has been shown that adding a zero-sequence component to the modulating signal in SM or changing the apportioning factor in SVM leads to the shift of pulse positions in output line voltages within a switching period and that, in both cases, the waveform of the ripple voltage and the amplitude of the ripple current are affected [8, 10]. The relation between v_h and μ, for each Sector is given by [14]

$$v_h = E(\frac{1}{2} - \mu) - (1 - \mu)v_x^* - \mu v_z^*. \qquad (1)$$

where for the reference voltages v_1^*, v_2^*, v_3^*, $v_x^* = \max\{v_1^*, v_2^*, v_3^*\}$ and $v_z^* = \min\{v_1^*, v_2^*, v_3^*\}$, within the modulating interval.

When introduced to (1), constant values of μ imply in NSMS as those indicated by $\mu = 0.5$ ($\mu_{1/2}$), $\mu = 0$, and $\mu = 1$ in Fig. 2(a). However, when μ varies alternately between 0 and 1, as a function of time, only discontinuous NSMS are obtained, as those indicated by $\mu = c(t)$, $\mu = \overline{c}(t)$, $\mu = d(t)$ and $\mu = \overline{d}(t)$, in Fig. 2(b). Consider $\theta_s = \omega_m t$ as the angle of the reference vector, with an angular

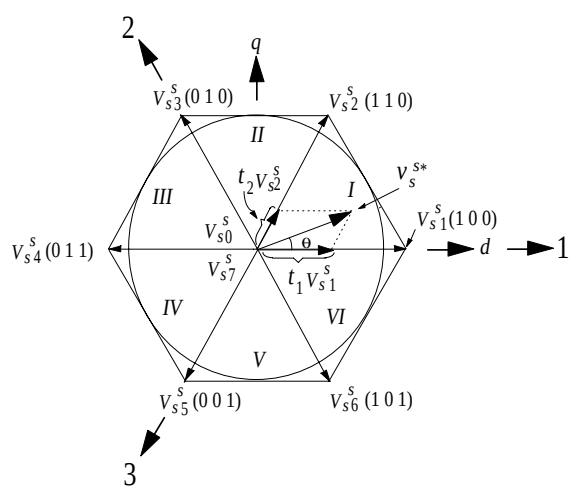

Fig. 1 Space vector plane

speed ω_m, in a given sector. In general, by considering all possibilities of discontinuous modulation, four types of behaviour of signal μ does occur. In the first type (Type μ_{00}) $\mu = 0$ during all the interval, that is for $\theta_s = \pi/3$ degrees. This is the case for strategies $\mu = 0$ and $\mu = c(t)$. In Type μ_{11}, $\mu = 1$ within the whole interval (e.g. with strategies $\mu = 1$ and $\mu = \overline{c}$). In the two other types the value of μ changes either from 0 to 1 (Type μ_{01}, or $\mu = d$) or from 1 to 0 (Type μ_{10}, or $\mu = \overline{d}$) at $\theta_s = \pi/6$. Reference [11] has shown that these types can be combined along the 360 degrees originating other PWM strategies.

III. RMS VALUE OF THE CURRENT ERROR

Although the Total Harmonic Distortion (THD) has been used as a comparison criterion among the different PWM strategies, the current ripple RMS is single-phase for measuring losses [3, 15]. In this proposed paper the amplitude of the ripple current is calculated as a function of the apportioning factor, being based on the concept presented in [16]. The advantage of the approach over other existing methods is to obtain a general expression for all PWM strategies. Next the principle of the approach is explained.

1) *Current ripple per phase*: Consider the single-phase inverter in Fig. 3(a) of which the load model load is that of Fig. 3(b). In fact, such model corresponds to the high frequency per phase model of an induction motor. The output voltage of the inverter, $v(t)$, is a pulsed waveform assuming either the value $+E/2$ or $-E/2$. The difference $\Delta v(t) = v(t) - v^*(t)$, where $v^*(t)$ is the reference voltage demanded at the inverter output, causes a current ripple $\Delta i(t)$ that depends on the load inductance L. Therefore,

$$\frac{d\Delta i(t)}{dt} = \frac{v(t) - v^*(t)}{L} = \frac{\Delta v(t)}{L} \tag{2}$$

represents the slope of the line segments describing $\Delta i(t)$, as shown in Fig. 3(c). If the switching frequency, f_s, is much greater than the output frequency, f_m, the reference voltage, $v^*(t)$, can be supposed to be constant during the switching interval, T_s. From Fig. 3(c), it can be shown that

$$T^+ = \frac{\Delta i^+ - \Delta i^-}{E/2 - v^*} L = \frac{\delta i(t)}{E/2 - v^*} L \tag{3}$$

where T^+ is the interval of time of Δi increase and $\delta i(t)$ is the difference between the positive and negative peaks of $\Delta i(t)$.

Also, it can be shown that the interval of Δi decrease, T^-, is given by

$$T^- = \frac{\delta i(t)}{E/2 + v^*} L \tag{4}$$

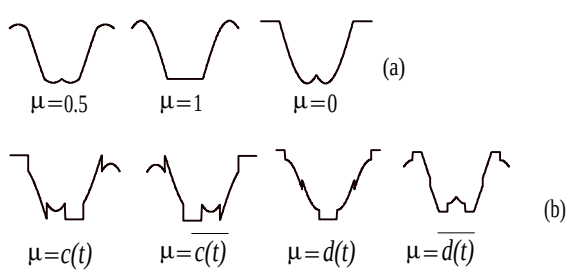

Fig. 2 Non-sinusoidal waveforms

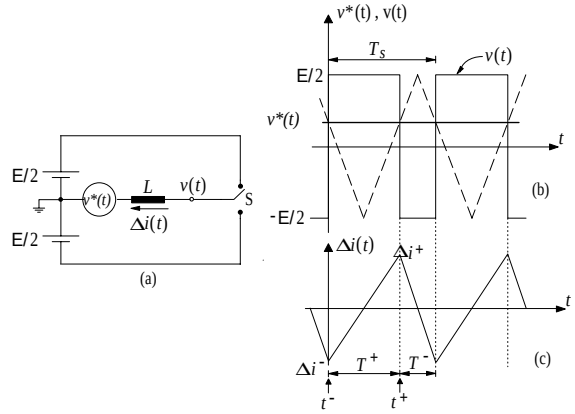

Fig. 3 Current ripple for a single-phase inverter

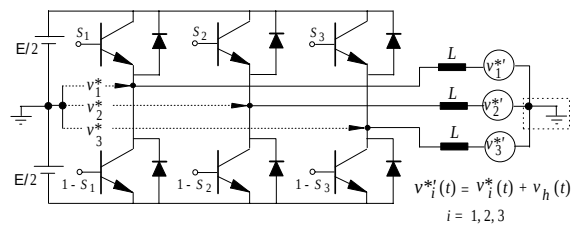

Fig. 4 Three-phase inverter

Since $T_s = T^+ + T^-$, $\delta i(t)$ can be calculated from equations (3) and (4) as

$$\delta i(t) = \frac{E^2 - 4v^{*2}}{4ELf_s} \tag{5}$$

2) *Current ripple for a three-phase inverter:* Consider now the three-phase in Fig. 4. Since in a three-phase inverter zero sequence components can be added to the reference voltages $v_j^*(t), j = 1, 2, 3$, the distorted voltage references can be represented by $v_j^{*'}(t) = v_j^*(t) + v_h(t)$. Therefore, for a three-phase inverter, the amplitude of the current ripple can be given by

$$\delta i(t) = \frac{E^2 - 4[v^{*\prime}]^2}{4ELf_s} \tag{6}$$

The transformation of $\delta i_i(t), i = 1, 2, 3$ into $\alpha\beta$ components, gives, δi_α and δi_α, is given by

$$\begin{bmatrix} \delta i_\alpha \\ \delta i_\beta \end{bmatrix} = \sqrt{\frac{2}{3}} \begin{bmatrix} 1 & -\frac{1}{2} & -\frac{1}{2} \\ 0 & -\frac{\sqrt{3}}{2} & \frac{\sqrt{3}}{2} \end{bmatrix} \begin{bmatrix} \delta i_1 \\ \delta i_2 \\ \delta i_3 \end{bmatrix}. \tag{7}$$

It can be shown, after some mathematical work, that for a modulation index m [17]

$$\delta i_\alpha = -\sqrt{\frac{3}{2}} \frac{\mathsf{m}}{Lf_s} [v_h(t) \cos \omega_m t + \frac{\mathsf{m}E}{8} \cos 2\omega_m t] \tag{8}$$

$$\delta i_\beta = \sqrt{\frac{3}{2}} \frac{\mathsf{m}}{Lf_s} [v_h(t) \sin \omega_m t - \frac{\mathsf{m}E}{8} \sin 2\omega_m t] \tag{9}$$

From equations (8) and (9) the RMS value of amplitude of the ripple current, $\delta i_{\alpha\beta}^2 = \delta i_\alpha^2 + \delta i_\beta^2$ can be calculated

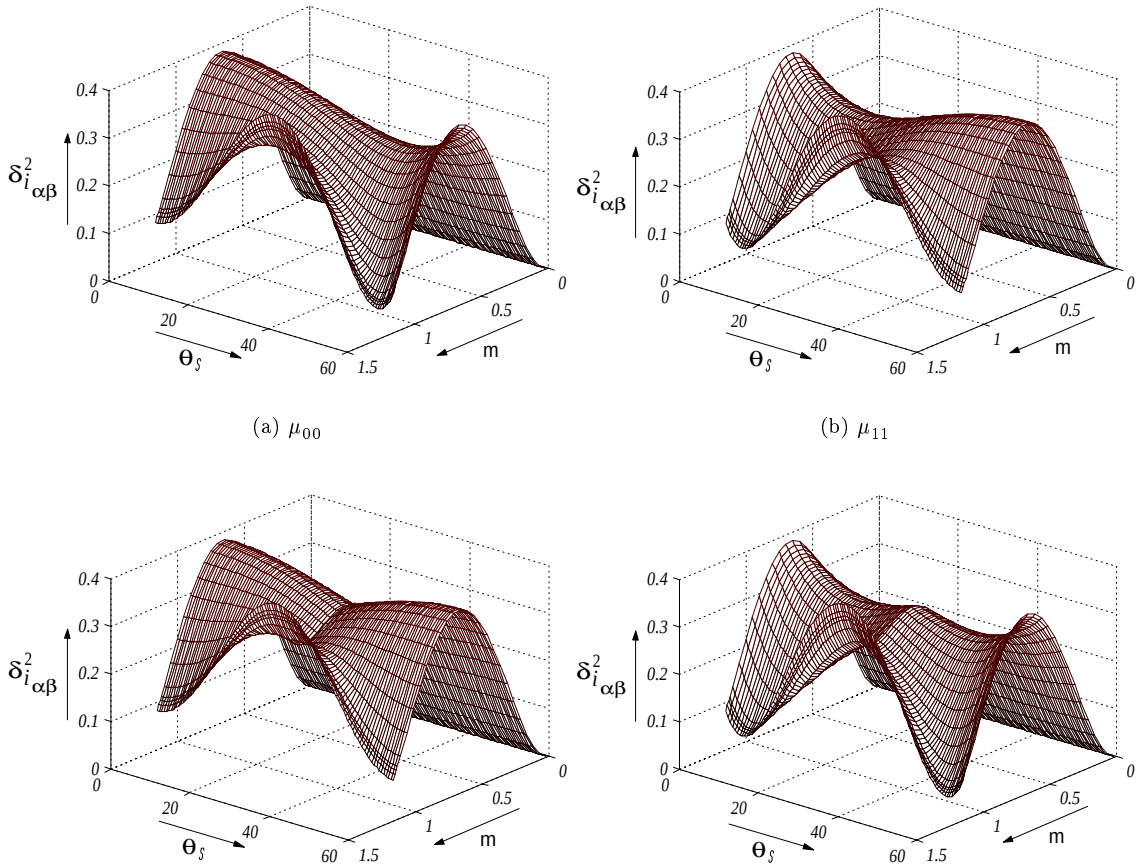

(a) μ_{00} (b) μ_{11}

(c) μ_{01} (d) μ_{10}

Fig. 5 Behaviour of $\delta^2 i_{\alpha\beta}$ non-sinusoidal strategies.

for the continuous and discontinuous modulation with a modulation index m, that is,

$$\delta i^2_{\alpha\beta} = k^2_{\mathsf{m}} \left(\frac{\mathsf{m}^2 E^2}{64} + v_h^2(t) + \frac{\mathsf{m}E}{4} v_h(t) \cos 3\omega_m t \right) \quad (10)$$

By substituting (1) in (10) for specific values of μ and m, in the interval of variation of θ_s, the $\delta i^2_{\alpha\beta}$ corresponding to the four Types discussed above for Sector I ($v_1^* > v_2^* > v_3^*$) can be calculated. They are shown in Fig. 5. It should be noticed that the behaviour of μ is the same at Sectors I, III and V and complementary at Sectors II, IV and VI.

The RMS value of amplitude of the current ripple in one sector can be obtained, for the continuous and discontinuous modulation, from

$$i^2_{RMS} = \frac{1}{\theta_{s\max}} \int_0^{\theta_{s\max}} \delta i^2_{\alpha\beta} d\theta_s. \quad (11)$$

where $\theta_{s_{\max}} = \pi/3$.

When applied to the four types of discontinuous modulation techniques $\mu_{00}, \mu_{11}, \mu_{01}$,and μ_{10} it gives

$$i^2_{RMS\mu_{00}} = \frac{k_{\mathsf{m}}}{8} \left[\frac{3\mathsf{m}^2 \left(1 + \frac{\sqrt{3}}{2\pi}\right)}{16} - \frac{\sqrt{3}\mathsf{m}}{\pi} + \frac{1}{3} \right], \quad (12)$$

$$i^2_{RMS\mu_{11}} = i^2_{RMS\mu_{00}} \quad (13)$$

$$i^2_{RMS\mu_{01}} = \frac{k_{\mathsf{m}}}{8} \left[\frac{\mathsf{m}^2 \left(3 + \frac{\sqrt{3}}{\pi}\right)}{16} - \frac{5\mathsf{m}}{3\pi} + \frac{1}{3} \right]. \quad (14)$$

$$i^2_{RMS\mu_{11}} = \frac{k_{\mathsf{m}}}{8} \left[\frac{\mathsf{m}^2 \left(3 + \frac{2\sqrt{3}}{\pi}\right)}{16} + \frac{\mathsf{m}(5/3 - 2\sqrt{3})}{\pi} + \frac{1}{3} \right].$$

with

$$k_{\mathsf{m}} = \left(\frac{3\mathsf{m}E}{RLf_m} \right)^2 \quad (15)$$

For the purpose of comparison the approach was applied to some continuous modulation techniques. When applied to the 3rd harmonic injection technique, i^2_{RMS} can be calculated as a function of the distortion index q, that is,

$$i^2_{RMS} = k\frac{\mathsf{m}^2}{48}(q^2 - \frac{q}{2} + \frac{1}{8}). \quad (16)$$

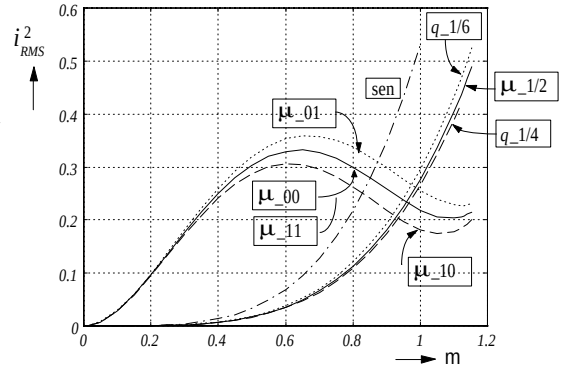

Fig. 6 Comparison of $\delta^2 i_{\alpha\beta}$ for continuous and discontinuous strategies

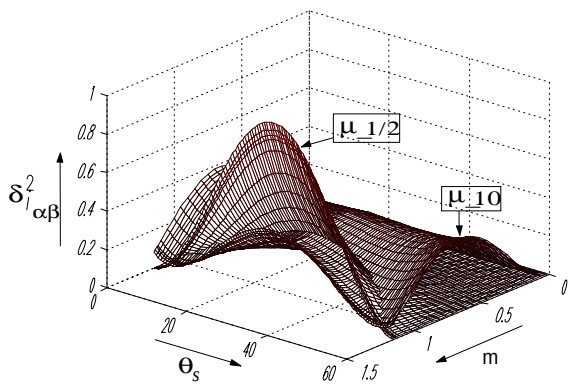

Fig. 7 Behaviour of $\delta^2 i_{\alpha\beta}$ for the combination of strategies $\mu_{1/2}$ and μ_{10}

From this expression it can be easily shown that minimum losses are achieved for $q = 1/4$, value also found in [18] by numerical methods. For the purpose of comparison the values $q = 0$ and $q = 1/6$ (referred here as *sen* and $q_{1/6}$, respectively) as well as the symmetrical vector modulation ($\mu_{1/2}$) have been examined.

A. High performance modulator

Different studies have used i^2_{RMS} as a criterion to compare continuous and discontinuous modulation [3, 15]. The strategies, $\mu_{00}(\mu = 0$ and $\mu = c)$, μ_{11} $(\mu = 1$ and $\mu = \overline{c})$, μ_{01} $(\mu = d)$ or μ_{10} $(\mu = \overline{d})$ can be compared to continuous modulation by using the RMS value of amplitude of the ripple current, i^2_{RMS}, as a function of the modulation index m, as shown in Fig. 6. These results studies confirm that strategy $q_{1/4}$ is marginally superior to strategy $\mu_{1/2}$, as mentioned in [15]. Strategy $\mu_{1/2}$ is, however, easier to be implemented by the use of the technique introduced in [11]. It also confirms that in the high modulation range all discontinuous methods (of which the technique $\mu = \overline{d}$ is the best) are superior to $\mu = 0.5$. It confirms, in addition, that the change from $\mu = 0.5$ $(\mu_{1/2})$ technique to $\mu = \overline{d}$ (μ_{10}) technique, at a value of m between 0.9 and 1, is the best technique for minimizing the current ripple, of which the behaviour is shown in Fig. 7. This strategy, however, does not take into account the load power angle.

Figure 8 describes the behaviour of the effective frequency ratio, k_{freq}, between the switching frequencies for discontinuous and continuous modulation, against the

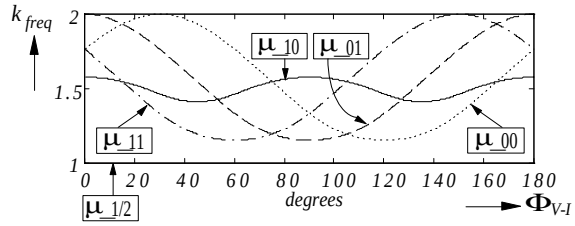

Fig. 8 Behaviour of k_{freq} as a function of the phase angle Φ_{V-I}

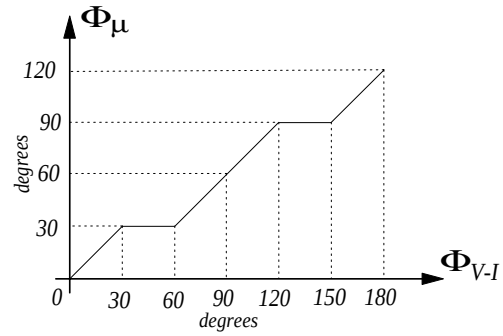

Fig. 9 Relation between Φ_μ and Φ_{V-I}

phase angle, Φ_{V-I}. It can be seen from that figure that for the technique μ_{10}, k_{freq} is maintained around 1.5 for all range of Φ_{V-I}. This is due to the voltage clamping for each phase during 1/3 of the fundamental period. But for $\Phi_{V-I} = 30$ degrees, for instance, $k_{freq} = 2$ if the technique μ_{00} is employed. This means that i^2_{RMS}, which is proportional to $1/k^2_{freq}$, reduces of 1/4, decreasing losses. For $\Phi_{V-I} = 0$ degree the technique to be chosen should be μ_{00}. For the PWM schemes, each output of the inverter legs can be alternately left on the positive or negative rail of the DC link for 120° intervals of the fundamental period [3]. In [19] the no switching region is allocated to $0^o \sim 60^o$ of the fundamental period because this range of phase lag is typical in practical applications of inverters. Extending this algorithm, the PWM scheme of [15] allocates the 60° interval of no switching region to $-60^o \sim 60^o$ of the fundamental period according to a given phase angle. These PWM schemes, however, do not guarantee the minimization of switching losses in all the range of the phase angle. This problem has been solved in [20], of which the technique is based on the space vector modulation and defines a modified voltage vector (referred to a general frame), of which the phase angle is a function of the actual phase angle. As a result the clamping segments of 60° are imposed to be in the vicinity of both the positive and negative current peak for a given power angle, Φ_{V-I}. Minimization of losses result from two factors: (a) low switching frequency ratio, and (b) absence of switching intervals in the vicinity of current peaks in a given phase.

Same technique is applied in this paper but with a difference in the use of the phase shift. A "modified power angle" Φ_μ, which is a function of μ, substitutes Φ_{V-I} in the method used by [20]. The relation between Φ_μ and Φ_{V-I} is given in Fig. 9. The subscript "μ" simply indicates that phase shift Φ_μ determines the behaviour of the apportioning factor μ. After the position of the modified reference voltage vector $v^*_{\Phi_\mu} = v^* e^{-j\Phi_\mu}$ is determined, the zero sequence component is calculated through (1).

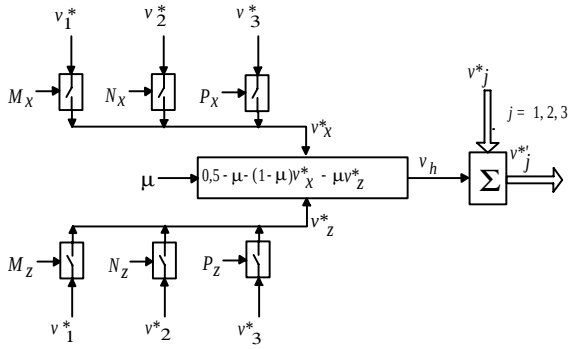

Fig. 10 PWM modulator for synthesizing the modulating signals specified by μ

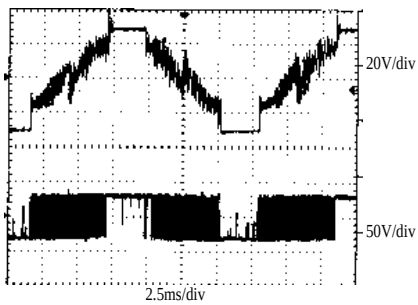

(a) μ_{00}

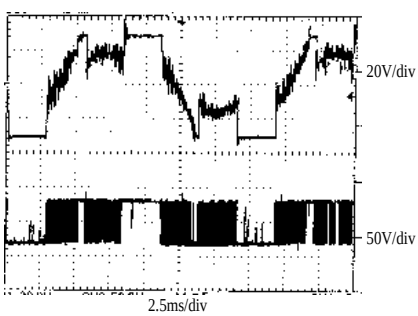

(b) μ_{10}

Fig. 11 Experimental results for the digital implementation.

B. Modulator implementation

The optimal technique presented above can be easily implemented by use of the modulator as described in [11, 14]. Such a modulator is based in the scheme indicated in Fig. 10, in the logic signal μ given by (1) determines the type of strategy to be implemented. These logic signals representing μ are obtained from the reference signals. The modulator can be implemented in either analog [11, 14] or digital version. In Fig. 11 experimental results for its digital implementation show the phase voltages for μ_{00} ($\mu = c$) and μ_{10} ($\mu = d$). Each figure also show the integration of the phase voltage, which results in the corresponding non-sinusoidal waveforms presented in Fig. 2.

The proposed technique imposes the clamping interval to be in the vicinity of the current maxima as requested by the phase angle of the load, Φ_{V-I}. This can be achieved if the signal $\mu = d$ is shifted as a function of Φ_μ, that is,

Table 1 Values of Φ_μ related to Φ_{V-I}.

Variação de Φ_{V-I}	Values de Φ_μ
$0° \longrightarrow 30°$	$\Phi_\mu = \Phi_{V-I}$
$30° \longrightarrow 60°$	$\Phi_\mu = 30°$
$60° \longrightarrow 120°$	$\Phi_\mu = \Phi_{V-I} - 30°$
$120° \longrightarrow 150°$	$\Phi_\mu = 90°$
$150° \longrightarrow 180°$	$\Phi_\mu = \Phi_{V-I} - 60°$

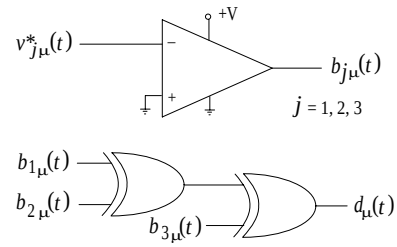

Fig. 12 Circuits that represent the operations resulting in the generation of d_μ

$d_\mu = d(t - \phi_\mu/\omega)$ for the law ϕ_μ vs Φ_{V-I} as described in Fig. 9. The expression that determine the shift values of ϕ_μ from Fig. 9 are given in Table 1.

By considering the set of three-phase signals

$$\begin{aligned} v_{1_\mu}^*(t) &= \cos(\omega_m t - \Phi_\mu) \\ v_{2_\mu}^*(t) &= \cos(\omega_m t - \frac{2\pi}{3} - \Phi_\mu) \\ v_{3_\mu}^*(t) &= \cos(\omega_m t + \frac{2\pi}{3} - \Phi_\mu). \end{aligned} \tag{17}$$

the logic signal d_μ can be obtained as shown Fig. 12.

Simulated results for $\Phi_{V-I} = 0^o$ to $\Phi_{V-I} = 105^o$ with increments of 15° are presented in Fig. 13(a) to (d) and Fig. 14(a) to (d). These results show that the 15° clamping intervals of phase "1" (full-line) are in the vicinity of the current peak in the same phase (dotted-line). Also, the behaviour of signal d_μ is included (dashed-line), the phase-shift Φ_μ being measured from the edge indicated by the arrow to the vertical dotted-line indicated in all figures. These results agree with those presented in [20]. It should be noticed that cases $\Phi_{V-I} = 0^o$ and $\Phi_{V-I} = 30^o$ to $\Phi_{V-I} = 60^o$ correspond to the experimental results in Fig. 11 for $\mu = d$ and $\mu = c$, respectively.

IV. CONCLUSION

The performance characteristics of different strategies have been examined in terms of the amplitude of the ripple current. Also, it has been confirmed the fact that reduced switching losses can be obtained by distributing the non-modulated segments in discontinuous PWM strategies along the fundamental period. This feature can be improved if the distribution of these segments varies accordingly to the phase angle between output voltage and current. Such technique has been easily implemented as a function of the apportioning factor by use of a hybrid modulator scheme that takes advantage of the correlation between carrier-based and space-vector modulation techniques. Simulated and experimental results corroborate the algorithm employed. An important point is that the modulation technique have been generated from simple

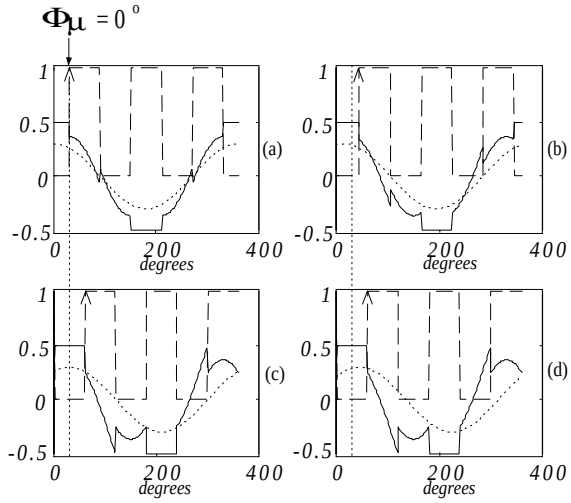

Fig. 13 Simulated results for the modulating signal (full trace), current phase (dotted trace) and logic signal used for implementation: (a) $\Phi_{V-I} = 0^o$ ($\Phi_\mu = 0^o$); (b) $\Phi_{V-I} = 15^o$ ($\Phi_\mu = 15^o$); (c) $\Phi_{V-I} = 30^o$ ($\Phi_\mu = 30^o$); (d) $\Phi_{V-I} = 45^o$ ($\Phi_\mu = 30^o$)

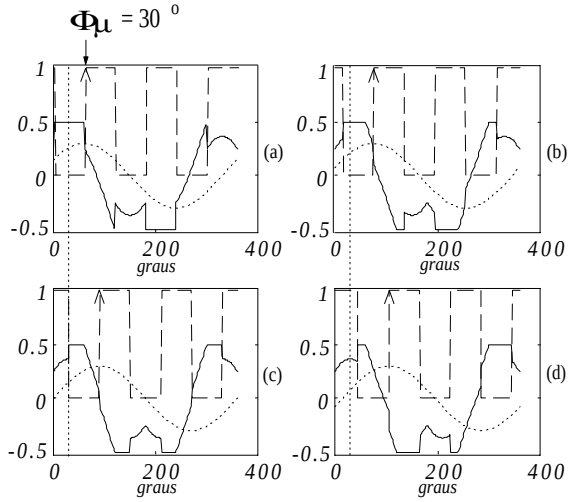

Fig. 14 Simulated results for the modulating signal (full trace), current phase (dotted trace) and logic signal used for implementation: (a) $\Phi_{V-I} = 60^o$ ($\Phi_\mu = 30^o$); (b) $\Phi_{V-I} = 75^o$ ($\Phi_\mu = 45^o$); (c) $\Phi_{V-I} = 90^o$ ($\Phi_\mu = 60^o$); (d) $\Phi_{V-I} = 105^o$ ($\Phi_\mu = 75^o$)

logic blocks, avoiding both hard calculation and the use of look-up tables.

REFERENCES

[1] L. Abraham and R. Blümel. Optimization of three phase pulse pattern by variable zero sequence component. In *Conf. Rec. EPE*, pages 272–277, 1991.

[2] H.W. van der Broeck, H.C. Skudelny, and G.V. Stanke. Analysis and realization of a pulsewidth modulator based on voltage space vectors. *IEEE Trans. Ind. Applicat.*, 24(1):142–150, jan/feb 1988.

[3] J. W. Kolar, H. Ertl, and F. C. Zach. Minimizing the current harmonics rms value of three-phase pwm converter systems by optimal and suboptimal transition between continuous and discontinuos modulation. In *Conf. Rec. PESC*, pages 372–381, 1991.

[4] H. Grotstollen. Line voltage modulation - a new possibility of pwm for three phase inverters. In *Conf. Rec. IAS Annual Meeting*, pages 567–574, 1993.

[5] A. Schönung and H. Stemmler. Static frequency changers with "subharmonic" control in conjuction with reversible variable-speed ac drives. *Brown-Boveri Review*, 51(1):555–577, aug/sep 1964.

[6] M. Depenbrock. Pulse width control of a 3-phase inverter with non-sinusoidal phase voltages. In *IEEE International Semiconductor Power Converter Conference*, pages 399–403, 1977.

[7] J.A. Houldsworth and D.A. Grant. The use of harmonic distorsion to increase the output voltage of a three-phase pwm inverter. *IEEE Trans. Ind. Applicat.*, 20(1):1224–1228, sep/oct 1984.

[8] D.G. Holmes. The significance of zero space vector placement for carrier based pwm schemes. In *Conf. Rec. IAS Annual Meeting*, pages 2451–2458, 1995.

[9] J. Sun and H. Grotstollen. Optimized space vector modulation and regular-sampled pwm: A reexamination. In *Conf. Rec. IAS Annual Meeting*, pages 956–963, 1996.

[10] V. Blasko. Analysis of a hybrid pwm based on modified space-vector and triangle-comparison methods. *IEEE Trans. Ind. Applicat.*, 33(3):756–764, may/jun 1997.

[11] R. N. C. Alves, E. R. C. da Silva, A. M. N. Lima, and C. B. Jacobina. Pulse width modulator for voltage-type inverters with either constant or pulsed dc link. In *Conf. Rec. IAS Annual Meeting*, pages 1229–1236, 1998.

[12] A. M. Hava, R. J. Kerkman, and T. A. Lipo. Simple analytical and graphical tools for carrier based pwm methods. In *Conf. Rec. PESC*, pages 1462–1471, 1997.

[13] D. W. Chung, J. S. Kim, and S. K. Sul. Unified voltage modulation technique for real time three-phase power conversion. In *Conf. Rec. IAS Annual Meeting*, pages 921–926, 1996.

[14] R.N.C. Alves, E.R.C. da Silva, and A.M. N. Lima. Pwm modulators for inverters with either constant or resonant dc link (in portuguese). In *Proceedings of the 4th Brazilian Power Electronics Conference(COBEP)*, pages 650–655, 1997.

[15] A. M. Hava, R. J. Kerkman, and T. A. Lipo. A high performance generalized discontinuous pwm algorithm. In *Conf. Rec. APEC*, pages 886–894, 1997.

[16] W. McMurray. Modulation of the chopping frequency in dc choppers and inverters having current-hysteresis controllers. *IEEE Trans. Ind. Applicat.*, 20(4):763–768, jul/aug 1984.

[17] R.N.C. Alves. *Analysis and implementation of pulse width modulation techniques for three phase inverters.* PhD thesis, UFPB/COPELE, 1998.

[18] S.R. Bowes and A. Midoun. Suboptimal switching strategies for microprocessor-controlled pwm inverter drives. *IEE Proceedings*, 132(3):133–148, may 1985.

[19] A.M. Trzynadlowski and S. Legowski. Minimum-loss vector pwm strategy for three-phase inverters. *IEEE Trans. Power Electron.*, 9(1):26–34, 1994.

[20] D. W. Chung and S. K. Sul. Minimum-loss pwm strategy for 3-phase pwm rectifier. In *Conf. Rec. PESC*, pages 1020–1026, 1997.